Developmental Biology 399 (2015) 2–14

Contents lists available at ScienceDirect

Developmental Biology

journal homepage: www.elsevier.com/locate/developmentalbiology

Loss of Npn1 from motor neurons causes postnatal deficits independent from Sema3A signaling

Michaela S. Helmbrecht [a,*,1], Heidi Soellner [a,1], Anna M.L. Truckenbrodt [a], Julia Sundermeier [a], Christian Cohrs [c,d], Wolfgang Hans [c], Martin Hrabě de Angelis [c,e,f], Annette Feuchtinger [b], Michaela Aichler [b], Karim Fouad [g], Andrea B. Huber [a,*]

[a] Institute of Developmental Genetics, Helmholtz Zentrum München, German Research Center for Environmental Health (GmbH), Ingolstaedter Landstr. 1, 85764 Neuherberg, Germany
[b] Research Unit Analytical Pathology, Insititute of Pathology, Helmholtz Zentrum München, German Research Center for Environmental Health (GmbH), Ingolstaedter Landstr. 1, 85764 Neuherberg, Germany
[c] German Mouse Clinic, Institute of Experimental Genetics, Helmholtz Zentrum Muenchen, German Research Center for Environmental Health (GmbH), Ingolstaedter Landstr. 1, 85764 Neuherberg, Germany
[d] DFG-Research Center for Regenerative Therapies Dresden, Technische Universität and Paul Langerhans Institute Dresden, German Center for Diabetes Research (DZD), Germany
[e] Chair of Experimental Genetics, Center of Life and Food Sciences Weihenstephan, Technische Universität München, 85354 Freising-Weihenstephan, Germany
[f] German Center for Diabetes Research (DZD), Ingostädter Landstr. 1, 85764 Neuherberg, Germany
[g] Faculty of Rehabilitation Medicine and Centre for Neuroscience, University of Alberta, Canada

ARTICLE INFO

Article history:
Received 28 August 2014
Received in revised form
24 November 2014
Accepted 25 November 2014
Available online 13 December 2014

Keywords:
Npn1
Sema3A
Motor neuron
Postnatal development

ABSTRACT

The correct wiring of neuronal circuits is of crucial importance for the function of the vertebrate nervous system. Guidance cues like the neuropilin receptors (Npn) and their ligands, the semaphorins (Sema) provide a tight spatiotemporal control of sensory and motor axon growth and guidance. Among this family of guidance partners the Sema3A-Npn1 interaction has been shown to be of great importance, since defective signaling leads to wiring deficits and defasciculation. For the embryonic stage these defects have been well described, however, also after birth the organism can adapt to new challenges by compensational mechanisms. Therefore, we used the mouse lines *Olig2-Cre;Npn1*^{cond} and *Npn1*$^{Sema-}$ to investigate how postnatal organisms cope with the loss of Npn1 selectively from motor neurons or a systemic dysfunctional Sema3A-Npn1 signaling in the entire organism, respectively. While in *Olig2-Cre*$^{+}$*;Npn1*$^{cond-/-}$ mice clear anatomical deficits in paw posturing, bone structure, as well as muscle and nerve composition became evident, *Npn1*$^{Sema-}$ mutants appeared anatomically normal. Furthermore, *Olig2-Cre*$^{+}$*;Npn1*^{cond} mutants revealed a dysfunctional extensor muscle innervation after single-train stimulation of the *N.radial*. Interestingly, these mice did not show obvious deficits in voluntary locomotion, however, skilled motor function was affected. In contrast, *Npn1*$^{Sema-}$ mutants were less affected in all behavioral tests and able to improve their performance over time. Our data suggest that loss of Sema3A-Npn1 signaling is not the only cause for the observed deficits in *Olig2-Cre*$^{+}$*;Npn1*$^{cond-/-}$ mice and that additional, yet unknown binding partners for Npn1 may be involved that allow *Npn1*$^{Sema-}$ mutants to compensate for their developmental deficits.

Introduction

The establishment of a precisely working nervous system is of crucial importance for all vertebrates in order to interact with their environment. Thus, during development billions of neurons have to extend axons towards their target regions and establish the proper connections, which they do in a highly specific manner and with stunningly few errors. To enable this high accuracy of axon growth and guidance those processes underlie tight spatiotemporal regulation by specific cues that allow for axon–axon interaction and communication of the axons with their environment (Huber et al., 2003). During the late embryonic and early postnatal phase the carefully established circuits then undergo several changes in the

* Corresponding authors.
E-mail addresses: michaela.helmbrecht@helmholtz-muenchen.de (M.S. Helmbrecht), andrea.huber@helmholtz-muenchen.de (A.B. Huber).
[1] Equal contribution

http://dx.doi.org/10.1016/j.ydbio.2014.11.024

process of circuit maturation, since axons compete for target derived trophic support. It is during this phase that misprojecting axons are identified and eliminated and synapses undergo activity-dependent modulation by potentiation or repression of their signals (Hensch, 2005; Lichtman and Colman, 2000; Vanderhaeghen and Cheng, 2010).

Since the development of well-functioning neuronal circuits is such a complex process it is of great interest how the organism as a whole can cope with axonal wiring defects after the initial phase of circuit establishment. In this respect we investigated the defects resulting from deficient signaling of the axon guidance cue Semaphorin 3A (Sema3A) and its receptor Neuropilin 1 (Npn1). This ligand–receptor interaction has been shown to play important roles in several distinct aspects of axon guidance, including timing of growth, selective fasciculation, and mediation of the interaction between sensory and motor axons (Huber et al., 2005; Huettl et al., 2011; Kolodkin and Tessier-Lavigne, 2011). Therefore, we used the mouse lines *Olig2-Cre; Npn1^{cond}*, in which the Npn1 receptor is specifically ablated from motor neurons, and *Npn1^{Sema-}*, where point mutations in the ligand-binding region of the receptor selectively abolish the interaction with Sema3A in the entire organism, however, without interfering with the interaction with VEGF receptor 2 (Gu et al., 2003).

During embryonic development, this interaction has been investigated intensively, especially in respect of its consequences on limb innervating motor axons of the lateral motor column (LMC). Thus, it has been shown that at E10.5 the interaction of this ligand–receptor pair prevents a precocious ingrowth of axons, since the repulsive ligand Sema3A is expressed in the entire limb mesenchyme. Later, the expression pattern of Sema3A changes and consequently a distinct path is cleared for the axons to guide their way through the developing limb in a surround repulsion manner (Huber et al., 2005; Kolodkin and Tessier-Lavigne, 2011). Accordingly, this signaling is responsible for the accurate timing of sensory and motor axon ingrowth into the limb. Subsequently, axon trajectories are determined by other interaction partners, like the ephrins and their Eph receptors (Egea and Klein, 2007; Kao et al., 2012), GDNF and its receptor c-Ret (Kramer et al., 2006), or Sema3F-Npn2 signaling (Huber et al., 2005), that work together in order to guide the developing axons through the limb to their appropriate targets in a stepwise manner. Given the important role of this interaction it is not surprising that its elimination leads to severe pathfinding deficits. Recent studies by Huettl et al., show that the conditional removal of Npn1 from sensory neurons affects the fasciculation of motor and sensory fibers while motor axon trajectories are still established correctly. In contrast, depletion of Npn1 specifically from motor neurons disrupts the fasciculation of motor axons. In these mutants also the dorsal–ventral pathfinding of motor axons is affected and the most advanced defasciculated motor projections hardly reach the distal forelimb (Huettl et al., 2011). In a former study by Huber et al., *Npn1^{Sema-}* mice were investigated and also here motor and sensory axons were defasciculated within the plexus even though individual nerve branches were still found in a roughly correct position distal to the plexus. Nevertheless, retrograde tracing from the ventral forelimb musculature also revealed dorsal–ventral pathfinding deficits of Npn1 expressing motor neurons. Additionally, these mice displayed deficits in sensory axon fasciculation and a precocious ingrowth of both, motor and sensory axons, into the limb (Huber et al., 2005). At later embryonic and early postnatal stages, defasciculation is still evident in intercostal and sciatic nerves in this mouse line (Haupt et al., 2010). Thus, while the embryonic defects resulting from the deficient Sema3A-Npn1 signaling are already well described, it is still unclear how the postnatal organism deals with these impairments and if the loss of connections can be balanced by compensational mechanisms.

In order to approach this question, we analyzed general health, bone structure, and muscle composition in *Olig2-Cre;Npn1^{cond}* mice and assessed the functionality of their brachial nerves by electrophysiological stimulation. Furthermore, we compared their nerve composition and their performance in several sensory and motor behavioral tests to that of mice of the *Npn1^{Sema-}* line. Our data suggest that loss of Sema3A-Npn1 signaling in motor neurons is not the only cause for the observed anatomical and functional deficits in *Olig2-Cre^{+};Npn1$^{cond-/-}$* mice and that additional, yet unknown binding partners for Npn1 may be involved in the wiring of the sensory-motor circuitry and compensate the developmental deficits in *Npn1^{Sema-}* mutants.

Material and methods

Ethic statement

Mice were handled according to the federal guidelines for the use and care of laboratory animals, approved by the Helmholtz Zentrum München Institutional Animal Care and Use Committee. All experimental procedures were approved by and conducted in adherence to the guidelines of the Regierung von Oberbayern.

Mouse lines (mus musculus)

The following mouse lines on a C57BL/6 background were used: *Hb9::eGFP* (Wichterle et al., 2002), *Npn1^{cond}* (Gu et al., 2003), *Npn1^{Sema-}* (Gu et al., 2003), *Olig2-Cre* (Dessaud et al., 2007). Genotyping was performed as described previously (Huettl et al., 2011). Since *Olig2-Cre^{wt};Npn1$^{cond-/-}$* and *Olig2-Cre$^{+/-}$;Npn1$^{cond\ wt}$* animals did not reveal any differences in their phenotype or motor neurons innervating the forelimb extensors (Fig. S1), only *Olig2-Cre^{wt};Npn1$^{cond-/-}$* animals were used as controls.

Electrophysiological analysis

Electrophysiological experiments were carried out in adult animals under Ketamine (0.1 mg/g, i.p., Bela-Pharm GmbH & Co. KG, Vechta, Germany) and Xylazine (0.01 mg/g, i.p., cp-pharma mbH, Burgdorf, Germany) anesthesia. An additional dose of anesthesia was given if required during the experiment. After the experiment, mice were euthanized without regaining consciousness.

The nerve stimulation procedure was modified from a previous protocol (Udina et al., 2008). The nerves of interest (i.e. *N. musculocutaneus, N. radial, N. median, N. ulnar*) were identified according to the literature (Greene, 1963) and stimulated with single bipolar electric pulses (100 μs duration) using custom made stimulation electrodes with 2 hooks (stainless steel, 0.2 mm in diameter with 1 mm in between). For the generation of the pulses the following instruments were used: Master-8 pulse generator, A.M.P.I, Jerusalem, Israel; Amplifier P511 DC; Astromed GmbH, Rodgau, Germany; Digidata 1440A Digitizer, Molecular devices, Sunnyvale, USA. Stimulation intensity was increased from 0 to 0.1 mA in 0.05 intervals (Isoflex-Flexible stimulus isolator, A.M.P.I). The elicited movement in the limb was described in terms of direction and body parts involved and afterwards compared between control and mutant animals.

Immunohistochemistry

For fluorescent immunohistochemistry tissue was fixed in 4% paraformaldehyde (PFA) overnight and cryoprotected in 30% sucrose. Spinal columns and arms of P0 animals were cryosectioned in 20 μm slices as series of 4. Spinal cords were sectioned at 40 μm sections using a sliding microtome (Leica) and every second section was analyzed. Immunohistochemistry was performed as described previously (Huber et al., 2005). For staining the following antibodies were used: rabbit anti-GFP (1:4000, Invitrogen), rat anti-myelin basic

protein (1:250, Biozol), mouse anti-myosin MY32 (1:400, Sigma-Aldrich), mouse anti-neurofilament 2H3 (1:50, obtained from the Developmental Studies Hybridoma Bank developed under the auspices of the NICHD and maintained by The University of Iowa, Department of Biological Sciences, Iowa City, IA 52242), rabbit anti-neurofilament 200 (1:1000, Sigma-Aldrich), and goat anti-Hsp27 (1:250, Santa Cruz). The staining was visualized with secondary antibodies conjugated to different fluorochromes (1:250; Molecular Probes; Jackson Dianova).

Alcian blue/Alizarin red differential staining of cartilage and bone

P0 mice were killed, skin removed, eviscerated and dehydrated in 100% EtOH for seven days followed by fixation in 100% acetone for 3 days. After brief washing in H_2O, mice were incubated in Alcian blue/Alizarin red staining solution (1 volume Alcian blue (Sigma-Aldrich), 1 volume Alizarin red (Sigma-Aldrich), 1 volume glacial acetic acid, 17 volumes EtOH) for 21 days with continual agitation. Remaining tissue was destained and macerated in 1% KOH, 20% glycerol at 37 °C for 24 h and subsequently stored at room temperature until tissue was destained. Skeletons were subjected to glycerol dilution series (20%, 50%, 80% in H_2O) and stored in 100% glycerol. Alcian blue/Alizarin red stained skeletons were imaged using a MZ APO stereomicroscope. Length and width of lower forelimb bone structures were quantified in pixels as measurement by ImageJ.

X-ray analysis

Dead mice were fixed on a plate permeable for X-rays and placed in the chamber of a MX-20 cabinet X-ray system (Specimen Radiography Systems, Illinois, USA). Images were taken and the parameters bone mineral content (BMC) and bone width were analyzed qualitatively using the NTB X-ray scanner (NTB GmbH, Diepholz, Germany) and the supplied iXPect software. Settings were Voltage: 25 kV and integration time: 40 ms.

Ultrastructural analysis of forelimb nerves

Adult animals were perfused transcardially with 1% phosphate buffered saline (PBS) for 5 min followed by fixation in 4% PFA and 0.25% glutaraldehyde in 0.1 M PB buffer (81 mM Na2HPO4, 19 mM NaH2PO4, pH7.4) for 10 min. Forelimb nerves *N.radial* and *N. median* were extracted, post-fixed overnight and subsequently stored in 2.5% glutaraldehyde in 0.1 M sodium cacodylate buffer (pH 7.4) (Electron Microscopy Sciences, Hatfield, USA) until embedding in epoxy resin. Ultrathin sections of nerve tissue were mounted on Formvar carbon coated copper grids for support prior to examination in an electron microscope EM 10 CR TEM (Zeiss, Jena, Germany). Single images were captured with a magnification of 5000 ×.

Individual EM images were arranged by multiple image alignment (MIA) to a single image representing the whole nerve cross-sectioned. These MIAs were subsequently quantified using the commercially available image analysis software Definiens Developer XD2 (Definiens AG, Munich, Germany) (Baatz et al., 2006; Baatz et al., 2009). Axons were classified into small diameter and large diameter fibers by a pixel threshold of 7000. The number of axons incorporated per Remak bundle was counted separately in individual EM images. Additionally, the *g*-ratio (axon diameter/fibre diameter) was calculated for each axon.

Retrograde labeling of motor neurons

At the age of 6 weeks, animals were anesthetized by i.p. injection of Ketamine (0.1 mg/g) and Xylazine (0.01 mg/g). Meloxicam (2 μg/g) was added as analgesic. The brachial plexus was exposed and 1 μl of the retrograde tracer cholera toxin subunit B, Alexa Fluor® 555 conjugate (CTB-A × 555) was injected into the required nerve. After 3 days, animals were perfused with PBS for 5 min and 4% PFA for 10 min, spinal cords were dissected, post-fixed overnight in 4% PFA and cryoprotected in 30% sucrose. 40 μm sections were cut with a sliding microtome and every second slice was used for analysis.

Behavioral data acquisition and analysis

Experimental design and housing

Testing of the animals was performed during the light phase of the light:dark cycle. Mice were housed under standard laboratory conditions in individually ventilated cages (Biozone Global, Kent, UK). All behavior data were measured by experimenters blinded to the genotype of the tested male mice and littermate controls.

Catwalk

For the analysis of specific gait parameters the Catwalk7.1 system (Noldus, Wageningen, Netherlands) was used (Glasl et al., 2012). The following settings were applied during data acquisition: Contrast (‰): 3990; Brightness × 0.001 V: -420; Pixel intensity threshold: 40; Pixel number threshold: 3. Since *Olig2-Cre*$^{+}$*;Npn1*^{cond} mutants did not traverse the glass plate voluntarily, these animals had to be air-puffed (referred to as “forced” conditions) to ensure a straight and continuous walk. Consequently, control littermates and mice of the *Npn1*$^{Sema-}$ line were likewise subjected to these “forced” conditions.

From the 6 runs videotaped during data acquisition, the 3 best were chosen based on the following criteria: comparable walking speed in the different runs, a minimum of 3 complete step cycles and a straight and continuous walk without stoppings. Runs were pre-processed with an analysis pixel threshold of 25 to differentiate unspecific background from paw prints before paw classification. The pixel areas of each paw print were classified manually as right or left fore- or hindlimb. The following parameters were used for analysis: Stand duration (s), Duty cycle and Usage of three paws.

Open field

4 weeks old male mice were tested for gross locomotion abnormalities in the open field apparatus (45.5 cm × 45.5 cm × 39.5 cm, TSE, Bad Homburg, Germany) in the dark during the light phase of the light:dark cycle for 20 min (Glasl et al., 2012). Recordings of the automated video-tracking system were analyzed with regard to horizontal (distance traveled) and vertical locomotion (number of rearings) parameters as well as average locomotor speed.

Ladder rung walking

The animals were subjected to cross a custom-made horizontal ladder with irregularly spaced round metal rungs and 2 side-walls of Plexi glass (74 cm length, 17 cm high walls of Plexi glass, 146 metal rungs of 1 mm diameter). The time to cross the ladder and the number of forelimb and hindlimb placement errors by either missing the rung or slipping of the rung was averaged over 3 successive trials (protocol modified from(Metz and Schwab, 2004)).

Rotarod

Mice were placed on a Rotarod apparatus (ROTA-ROD/RS, Bioseb, Vitrolles Cedex, France) continuously accelerating from 4 to 40 rpm in 2 min. The latency of the mice on the accelerating rod in rpm and seconds was recorded for 3 trials with 15 min inter-trial interval. The mice were stopped on the second passive rotation or when falling off the rod (Glasl et al., 2012).

Statistical analysis

All results were calculated as mean values SEM using Prism 5.0 software (GraphPad Software, La Jolla, USA). Anatomical data were analyzed with the Student's *t*-test or, in case of unequal variances, with the Student's *t*-test with Welch's correction. Behavioral data sets were initially checked for normal distribution with the D'Agostino–Pearson normality test. In case the data values deviate from a Gaussian distribution, single comparisons were computed with the non-parametric unpaired Mann–Whitney test. A *p*-Value less than 0.05 was set as statistical significance. Significant values were marked by *, *p*-Values below 0.01 by **, and highly significant *p*-Values lower than 0.001 by ***.

Results

During embryonic development, loss of the receptor Npn-1 from motor neurons causes severe defasciculation of motor axons accompanied by a reduction of their distal advancements, whereas sensory axons remain unaffected (Huettl et al., 2011). In contrast, in $Npn1^{Sema-}$ mice, in which the Sema3A-Npn1 signaling is abolished in all cells of the body, not only motor but also sensory projections are defasciculated (Huber et al., 2005). To investigate how these embryonic malformations affect the mice in their postnatal development and behavior both mouse lines were analyzed after birth.

Olig2-Cre^{+};Npn1$^{cond-/-}$ mice show abnormal forepaw posturing and growth retardation

At P0, *Olig2-Cre^{+};Npn1^{cond}* mutant pups revealed an atypical posturing of their forelimbs with constant flexion of one or both paws (Fig. 1A). This phenotype was completely penetrant in all mutants of this line, however, the degree of impairment was variable between the individuals with one or both paws being affected and differences in the severity of their posturing deficits. Interestingly, we never observed any abnormalities in the hindlimbs of these mice. Furthermore, the described phenotype persisted throughout postnatal development maintaining the grade of severity. Four days after birth also a significant decrease in weight became evident and mutants stay significantly lighter until adulthood (Figs. 1B and C). $Npn1^{Sema-}$ mutants display similar weight deficits (Fig. 1D), however, these animals never showed any abnormalities in limb posturing (data not shown).

Loss of functional innervation of extensor muscles in the forelimbs of Olig2-Cre^{+};Npn1$^{cond-/-}$ mice

Since the forelimb posturing defect that we observed in *Olig2-Cre^{+};Npn1$^{cond-/-}$* mutants is very reminiscent of the wrist-drop caused by radial nerve palsy (Reid, 1988), we aimed to analyze the functionality of the forelimb muscle innervation. For this purpose, we performed single train stimulation of the nerves in the brachial plexus and characterized the resulting movements (Table 1). The macroscopic organization of the brachial plexus was not altered in *Olig2-Cre^{+};Npn1$^{cond-/-}$* mutants (observations from 36 mutants and 38 control animals). Therefore, it was possible to identify individual nerves according to literature (Greene, 1963). Upon stimulation of the *N. radial* in control animals we observed an extension of wrist and digits. In contrast, in affected paws of *Olig2-Cre^{+};Npn1$^{cond-/-}$* mice extensor movements were never seen for any forelimb parts, instead a flexion in the elbow occurred. Stimulation of the other three major nerves in the brachial plexus, *N. median*, *N. ulnar* and *N. musculocutaneous*, which innervate the flexor muscles of the forelimb, evoked identical movements in mutant and control animals. Thus, we found functional deficits in the motor response of *Olig2-Cre^{+};Npn1$^{cond-/-}$* mutants that might be caused by a dysfunctional innervation of the forelimb extensor muscles due to embryonic axon wiring defects. However, to this point we were not able to exclude that muscle or bone deficits are involved in these impairments. Therefore, we investigated the musculoskeletal system in the next step.

Atrophy of the extensor muscle and postnatal bone malformations in affected forelimbs of Olig2-Cre^{+};Npn1^{cond} mutants

During development, motor axons extend towards the periphery in order to innervate their correct target muscles. Later, axons that did not reach their targets die due to the lack of trophic support (Hollyday and Hamburger, 1976) and muscles that are not innervated atrophy due to missing activity (Jolesz and Sreter, 1981). Therefore, we investigated, whether the wrist-drop in *Olig2-Cre^{+};Npn1^{cond}* mutants is accompanied by a atrophy of extensor musculature and analyzed the volume of specific muscles in the lower forearm (Fig. 2A). Already at birth, we observed a dramatic reduction of muscle volume for the extensor muscles *Extensor Carpi Radialis Longus* (ECRL) and *Extensor Carpi Radialis Brevis* (ECRB) in the mutants (−44% and −22%, respectively) when compared to wildtype littermates. This atrophy of extensor muscles is maintained until adulthood and detectable upon visual inspection. In contrast, the size of the control muscle *Flexor Carpi Ulnaris* (FCU) remained unchanged in these animals (Fig. 2A). In order to investigate if flexor muscles in more distal positions were affected, we also analyzed flexor muscles in the forepaws of these animals. However, the reduction in the total volume of the musculature did not reach significance (Fig. 2B). These data suggest that the described wrist drop is the result of an atrophy of forelimb extensors muscles that is caused by their dysfunctional innervation.

Due to the biomechanical link of muscles and bones, neuromuscular function has a direct impact on the properties and remodeling of bones during skeletal growth (Gross et al., 2010). Therefore, the bone and cartilage structure in affected forelimbs was analyzed at P0 and at 40 weeks of age using differential Alizarin Red S and Alcian blue staining and X-ray studies, respectively. At birth, the distribution of bone and cartilage, as well as bone thickness and length revealed no differences between mutant and control animals (Fig. 2C). However, at the age of 40 weeks digits and joints were deformed and radius and ulna bones were thinner and showed a lower density in mutants compared to their control littermates (Fig. 2D). These data indicate that neuromuscular dysfunction in *Olig2-Cre^{+};Npn1$^{cond-/-}$* mice causes bone malformation as a result of constant mechanical disuse.

Ultrastructural analysis of nerve fiber composition reveals abnormalities in the N. radial nerve of Olig2-Cre^{+};Npn1^{cond} mutants

Since the innervation of the forelimb extensor musculature was found to be dysfunctional in *Olig2-Cre^{+};Npn1^{cond}* mutants, we next investigated the nerves of the brachial plexus in closer detail. During embryonic development, the motor axons of these animals showed severe defasciculation and dorsal–ventral pathfinding deficits (Huettl et al., 2011). However, for a well-functioning neuronal circuit also the myelination and the axonal composition of the nerves are of crucial importance. In this aspect the proper interaction of developing peripheral axons with Schwann cells is necessary, in order to establish tight associations which are essential for the myelination of single large diameter axons and the coating of small unmyelinated axons in Remak bundles (Garbay et al., 2000; Jessen and Mirsky, 2005; Yu et al., 2005).

In order to investigate whether Npn1 plays a role in axon sorting and/or the axon–Schwann cell interaction, we analyzed the brachial nerves *N. radial* and *N. median* of adult mice ultrastructurally using

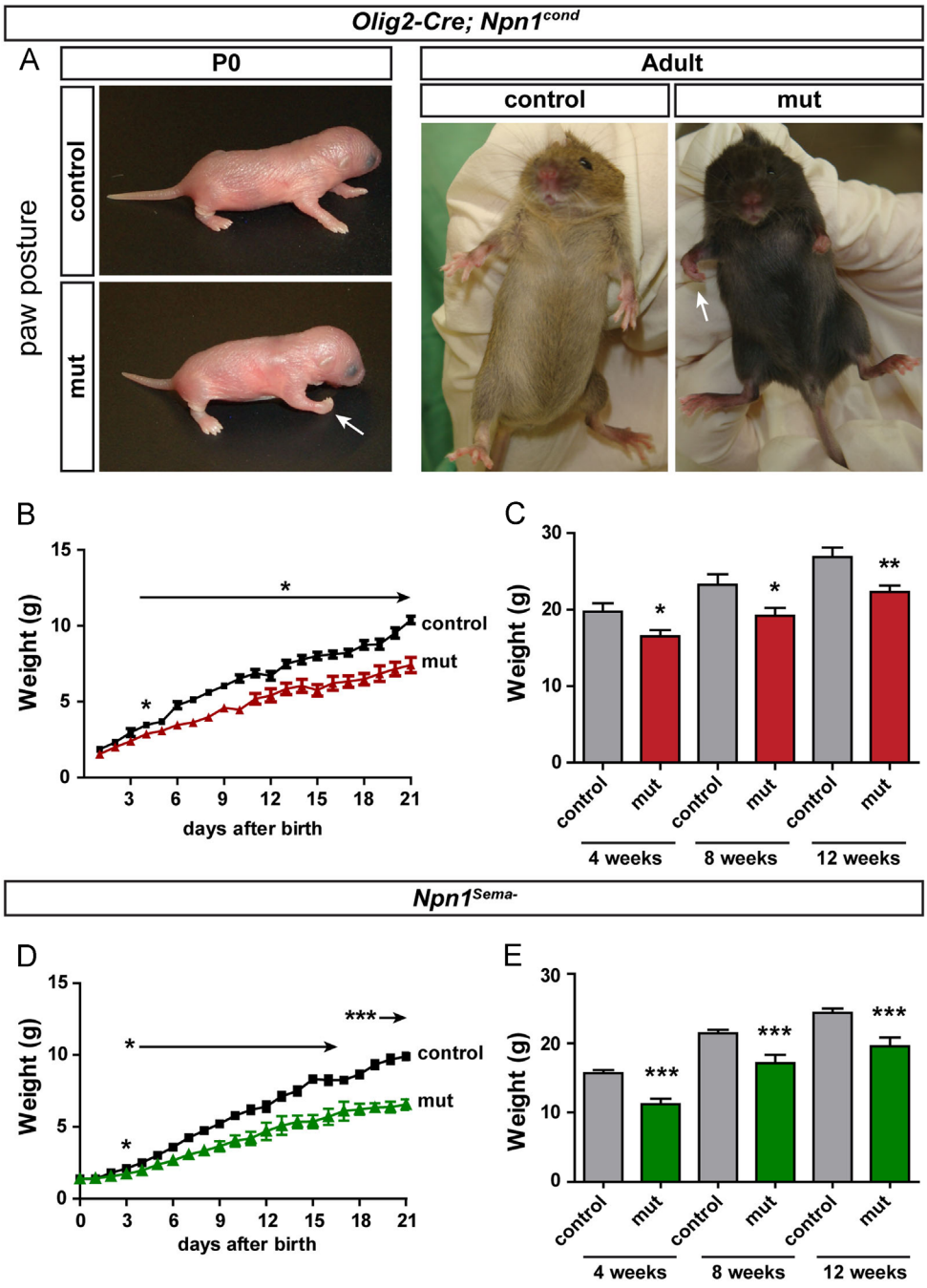

Fig. 1. Posturing deficits and growth retardation in *Olig2-Cre*$^{+}$;Npn1^{cond} mutants. (A) In *Olig2-Cre*$^{+}$;*Npn1*^{cond} mutants posturing deficits of the forelimbs (arrows) are evident already at birth and are retained until adulthood. (B) Starting at P4, mutants show a significantly decreased weight compared to controls (3.47 ± 0.20 g, $n=6$ vs. 2.87 ± 0.03 g, $n=3$, $p<0.05$), which becomes more evident in older animals (P21: 10.38 ± 0.25 g, $n=6$ vs. 7.42 ± 0.51, $n=6$, $p<0.001$). (C) The decreased weight of mutants is maintained until adulthood (4 weeks: 19.73 ± 1.08 g vs. 16.51 ± 0.81 g, $p=0.028$; 8 weeks: 23.25 ± 1.37 g vs. 19.20 ± 1.04 g, $p<0.05$; 12 weeks: 26.89 ± 1.22 g vs. 22.30 ± 0.84 g; $p<0.01$; $n=10$ for each time point). (D) *Npn1*$^{Sema-}$ mutants are significantly lighter compared to controls starting at postnatal day 3 (2.11 ± 0.06 g, $n=7$ vs. 1.73 ± 0.13 g, $n=4$, $p<0.02$), reaching highly significant levels at postnatal day 18 (8.66 ± 0.26 g, $n=10$ vs. 6.23 ± 0.38 g, $n=4$, $p<0.001$). (E) Also *Npn1*$^{Sema-}$ mutants maintain their reduced weight until adulthood (4 weeks: 15.70 ± 0.42 g, $n=37$ vs. 11.21 ± 0.79 g, $n=15$, $p<0.001$; 8 weeks: 21.40 ± 0.51 g, $n=35$ vs. 17.12 ± 1.22 g, $n=11$, $p<0.001$; 12 weeks: 24.38 ± 0.65 g, $n=32$ vs. 19.57 ± 1.27 g, $n=11$; $p<0.001$).

EM images (Fig. 3A). For this purpose, the *g*-ratio, as a relation of the thickness of the myelin sheath to the total axon diameter, served as a parameter for the myelination status of the nerves. Furthermore, the composition of the nerves regarding the amount of large and small diameter axons and the structure of the Remak bundles was analyzed.

In *Olig2-Cre;Npn1*^{cond} mice, the myelination of *N. radial* and *N. median* did not reveal any differences between the *g*-ratios of axons from control and mutant animals (Fig. 3B). However, in mutant animals, the *N. radial* contained a significantly reduced proportion of large diameter axons and a slightly increased proportion of small diameter axons. Also, the number of axons per Remak bundle was significantly elevated by a factor of 2.38 when compared to control littermates (Fig. 3B). Interestingly, for the control nerve *N. median* no changes in the axonal composition were found between mutant and wildtype littermates and also the number of axons per Remak bundle remained unaffected (Fig. 3B).

Since these data suggest a role for Npn1 in the process of axon sorting and for the interaction with Schwann cells it was of great interest to establish whether these effects are dependent on

Table 1
Abnormal limb movement after stimulation of the radial nerve of *Olig2-Cre^{+};Npn1^{cond} mutants*. Upon stimulation of the four major nerves of the brachial plexus flexor muscles appear to be innervated properly and show the same movements in mutants and control littermates. Stimulation of the radial nerve, that innervates the extensor muscles of the forelimb, results in abnormal movements of the limbs. Here, instead of an extension of the arm, the limb is flexed at the elbow ($n=3$ for both groups).

Nerve	Control	Mut
N. musculocutaneous	Flexion	Flexion
N. median	Flexion	Flexion
N. radial	**Extension**	**Flexion**
N. ulnar	Flexion	Flexion

Sema3A-Npn1 signaling. Therefore, we studied the composition of these nerves in *Npn1^{Sema-}* mutants in which the semaphoring binding site of the Npn1 receptor is destroyed (Gu et al., 2003). Interestingly, these mice did not reveal any abnormalities in myelination of the axons and the distribution of axons and Remak bundles in the *N. radial* did not show any obvious changes in the mutants compared to their wildtype littermates (Fig. 3C).

Thus, our data propose a shift in the ratio of small and large diameter axons and an increase in the amount of axons incorporated per Remak bundle in the *N. radial* caused by the absence of Npn1 in motor neurons. However, the missing Sema3A-Npn1 signaling seems not to be the reason for these changes, since myelination and nerve fiber composition is not affected in *Npn1^{Sema-}* mutants.

Alterations in the nerve composition of Olig2-Cre^{+};Npn1^{cond} mutants are due to a loss of motor axons

Next, we investigated if the shift from large to small diameter axons in the *N. radial* of *Olig2-Cre^{+};Npn1^{cond}* mutants was caused by a reduction of the axon diameter or if the distribution of motor and sensory axons is affected in these animals. Therefore, we crossed our mice with a line that expresses the genetic marker *Hb9::eGFP* to obtain animals in which motor neurons and their axons are labeled by the expression of GFP (Wichterle et al., 2002). *N. radial* and *N. median* were dissected from the brachial plexus and the composition of the nerves was analyzed with immunohistochemical stainings of their cross-sections (Fig. 4A). In *Olig2-Cre^{+};Npn1$^{cond-/-}$; Hb9::eGFP^{+}* mutant animals, we found a highly significant decrease of 53.6% for the size of the *N. radial* and of 33.8% for the *N. median* when compared to wildtype littermates. Furthermore, the relative nerve composition of the *N. radial* was significantly altered with a strong reduction in the proportion of motor axons and a significant increase in the number of sensory axons per μm^2. None of these alterations were found for the control nerve *N. median* (Figs. 4B) (for total number of axons per section see Fig. S2). Even though the relative amount of sensory axons was increased in the *N.radial*, their total number was significantly reduced (Figs. S2 and S3A). This effect was, however, not caused by a specific loss of sensory innervation, as the composition of sensory neurons in the dorsal root ganglia was not changed (Figs. S3B andS3 C). In *Npn1^{Sema-}; Hb9::eGFP^{+}* mutants the size and the composition of the *N. radial* were not affected (Fig. 4C).

Since these results depended on the expression of GFP under the promotor of the embryonic motor neuron marker Hb9 and it is not clear if expression levels are altered in postnatal animals, we confirmed the result by an alternative approach independent from GFP expression levels. For this purpose, we performed retrograde tracings directly from the nerves in the brachial plexus (Fig. 5A) and quantified the total number of motor neurons in the brachial spinal cord using GFP and Hsp27 as alternative motor neuron markers (Plumier et al., 1997)(Fig. S4A). For *Olig2-Cre^{+};Npn1^{cond}* mutants the number of retrogradely labeled motor neurons of the *N. radial* was significantly decreased by one fourth, while for the *N. median* no significant reduction in the number of traced motor neurons was detectable (Fig. 5B). In contrast, for mutants of the line *Npn1^{Sema-}* no difference in the number of retrogradely labeled motor neurons was found (Fig. 5C). In both lines the total number of motor neurons was not affected for either of the two markers GFP and Hsp27 (Figs. S4B and S4C).

Complex motor skills, but not sensory function, are impaired in Olig2-Cre^{+};Npn1^{cond} mutants

In order to investigate, whether the anatomical deficits that we have described in *Olig2-Cre^{+};Npn1^{cond}* mutants affect these animals. We performed several behavioral tests for motor function. In addition, we analyzed *Npn1^{Sema-}* mice that also show deficits in motor innervation and defasciculation of motor projections during embryonic development. Moreover, in *Npn1^{Sema-}* mutants also sensory axons were found to be defasciculated, which was not the case for *Olig2-Cre^{+};Npn1$^{cond-/-}$* mice (Huber et al., 2005; Huettl et al., 2011).

First, the general locomotor activities of both mouse lines were analyzed in an open field arena. In order to exclude possible anxiety related effects on gross locomotion, mice were tested in the dark during the light phase of the light:dark cycle (Zadicario et al., 2005). Within a time frame of 20 min, the locomotion speed and the total distance that was traveled by the animals were measured and used as parameters. Surprisingly, despite the posturing abnormalities and the anatomical changes in *Olig2-Cre^{+};Npn1^{cond}* mutants, we found no deficits in horizontal locomotion and also the velocity of their movements was comparable to their littermate controls (Fig. 6A). All parameters were slightly decreased for mutants, however, none of them reached a significant level. Also *Npn1^{Sema-}* mutants revealed no significant changes in their locomotor capabilities (Fig. 6A).

Since gross overground locomotion was not affected in *Olig2-Cre^{+};Npn1$^{cond-/-}$* mice, more complex motor skills were tested next. Here, the animals were tested repetitively at 4, 8 and 12 weeks of age to monitor any postnatal amelioration or deterioration.

The accelerating rotarod test allows for assessing the balance and endurance of animals by measuring the fall latency. Here, impairments in balance for *Olig2-Cre^{+};Npn1^{cond}* mutants at the age of 4 weeks became evident, since their latency on the rod was reduced to approximately half the time as for their control littermates (Fig. 6B). Interestingly, for these mutants we found no changes in their performance on the rotarod from 4 to 12 weeks of age. In contrast, *Npn1^{Sema-}* animals performed at wildtype levels at each time point tested (Fig. 6B).

For the analysis of forelimb–hindlimb coordination, the ladder rung walking test was chosen. On the horizontal ladder with irregular bars, *Olig2-Cre^{+};Npn1^{cond}* mutants needed significantly more time for the crossing compared to their control littermates and they showed no improvement in this task from 4 to 12 weeks of age (Fig. 6C). In this test also *Npn1^{Sema-}* mutants performed significantly worse than the controls at the age of 4 weeks. Interestingly, over the next 8 weeks these mutants were able to improve their performance, so that at the age of 12 weeks no significant difference to wildtypes was detectable (Fig. 6C).

To investigate the movement of *Olig2-Cre^{+};Npn1$^{cond-/-}$* mice in more detail, their gait was analyzed with the CatWalk7.1 gait analysis system. The system allows for the analysis of multiple gait parameters and enables a detailed assessment of the locomotion of the animals. Thus, for *Olig2-Cre^{+};Npn1^{cond}* mutants the phases in which they use three paws at the same time were increased by 40.5% compared to controls. Moreover, the stride length of fore- and hindpaws was shortened by 29.7% and 23.3%, respectively, and

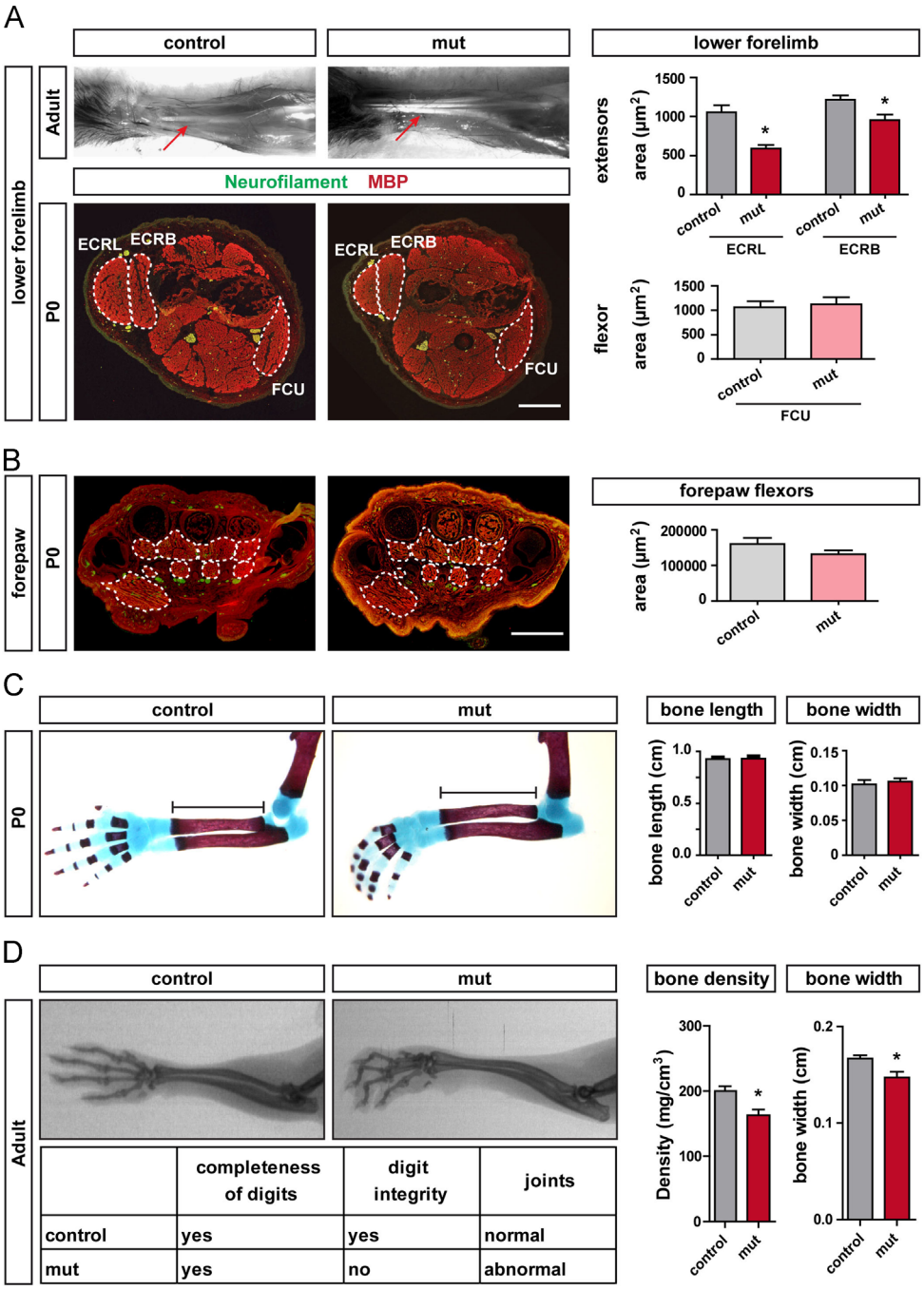

	completeness of digits	digit integrity	joints
control	yes	yes	normal
mut	yes	no	abnormal

Fig. 2. *Olig2-Cre*$^{+}$*;Npn1*^{cond} mutants reveal muscle atrophy and bone malformation. (A) In adult *Olig2-Cre*$^{+}$*;Npn1*^{cond} mutants extensor muscles of the forelimb are severely atrophied, revealing tendons that are usually located beneath (red arrows). This muscular atrophy becomes already evident at birth, when *Olig2-Cre*$^{+}$*;Npn1*^{cond} mutants show a significant reduction of muscle size in the extensors of the lower forearm extensor carpi radialis longus (ECRL) and extensor carpi radialis brevis (ECRB) compared to control animals (ECRL: $1053 \pm 92.06\ \mu m^2$ vs. $588.8 \pm 48.70\ \mu m^2$, $p < 0.05$, $n=3$; ECRB: $1215 \pm 56.49\ \mu m^2$ vs. $951.6 \pm 72.55\ \mu m^2$, $p < 0.05$, $n=3$). In contrast, the flexor musculature of the forearm flexor carpi ulnaris (FCU) ($1061 \pm 121.7\ \mu m^2$ vs. $1121 \pm 143.1\ \mu m^2$, $p=0.77$, $n=3$) is not affected. Scale bar: 50 µm. (B) The total area of the paw musculature shows no significant difference between mutants and controls ($160600 \pm 16450\ \mu m^2$ vs. $131300 \pm 7562 \mu m^2$, $p=0.11$, $n=4$). Scale bar 50 µm. (C) At P0, bone size of mutants does not show any significant alteration when compared to controls (length: 0.926 ± 0.009 cm vs. 0.930 ± 0.015, $p=0.82$, $n=4$; width: 0.101 ± 0.007 cm vs. 0.106 ± 0.004, $p=0.61$, $n=4$). (D) In adult mutants (40 weeks), joints and digit integrity showed morphological abnormalities. Density (200.0 ± 7.72 mg/cm^3, $n=6$ vs. 163.0 ± 8.96 mg/cm^3, $n=4$, $p < 0.02$) and thickness (0.167 ± 0.0032 cm, $n=6$ vs. 0.147 ± 0.0062 cm, $n=4$, $p < 0.02$) of the radius bone were significantly reduced in *Olig2-Cre*$^{+}$*;Npn1*^{cond} mutants.

the duty cycle, which represents the walking rhythm as a percentage of the standing time in the whole step cycle, was significantly decreased (Fig. 6D). These data suggest that *Olig2-Cre*$^{+}$*;Npn1*^{cond} mutants show irregularities in their gait due to the impairments of their affected forelimbs. Furthermore, the forelimb posturing deficits account for characteristic paw prints. In contrast, mice of the line *Npn1*$^{Sema-}$ displayed no significant alterations in any of these parameters (Fig. 6D).

These data suggest that only skilled motor functions but not gross locomotion or sensory function are affected by the loss of Npn1 from motor neurons. Furthermore, the loss of Sema3A-Npn1 signaling seems to be not the only cause for these impairments, since mutants of the *Npn1*$^{Sema-}$ line are less affected in all tests and can improve their performance over time.

In summary, our data show that *Olig2-Cre*$^{+}$*;Npn1*^{cond} mutants suffer from atrophy in the extensor muscles of the lower forearm

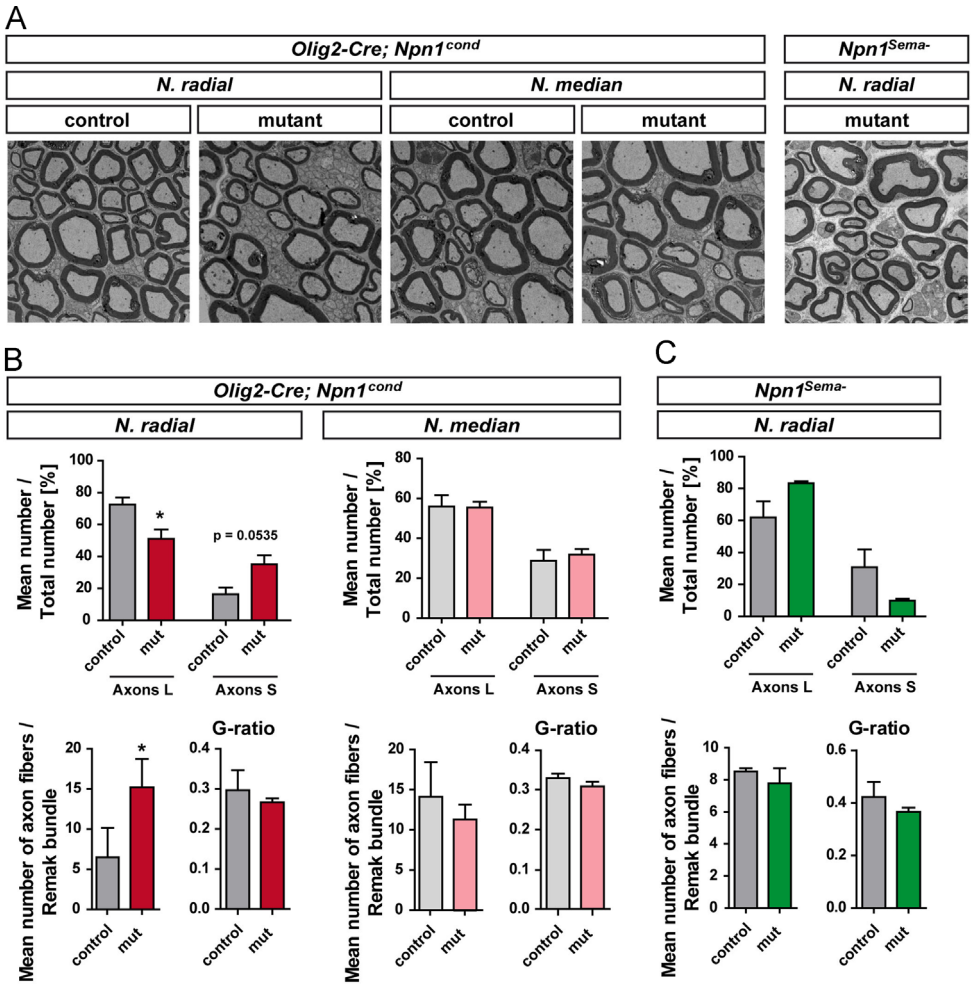

Fig. 3. Composition of the radial nerve is altered in *Olig2-Cre*$^{+}$*;Npn1*^{cond} mutants. (A) Representative images of the nerve composition visualized by electron microscopy. Magnification: 5000×. (B) The radial nerve *of Olig2-Cre*$^{+}$*;Npn1*^{cond} mutants reveals a significant reduction of large diameter axons (72.55% ± 4.38% vs. 51.14% ± 5.78%, $n=3$, $p<0.05$) and an increase of small diameter axons which remains not significant (16.38% ± 4.17% vs. 35.16% ± 5.53%, $n=3$, $p=0.053$). Furthermore, the mean number of axons per Remak bundle is significantly increased (6.494 ± 2.11 vs. 15.20 ± 2.03, $n=3$, $p<0.05$). The *G*-ratio remains unchanged (0.297 ± 0.050 vs. 0.266 ± 0.010, $n=3$, $p=0.58$). In contrast, no significant changes are evident for the composition of the median nerve (large diameter axons: 55.94% ± 5.68% vs. 55.40% ± 2.92%, $n=3$, $p=0.94$; small diameter axons: 28.75% ± 5.39% vs. 31.85% ± 2.79%, $n=3$, $p=0.64$; axons per Remak bundle: 10.46 ± 1.87 vs. 8.342 ± 0.80, $n=3$, $p=0.35$; *G*-ratio: 0.330 ± 0.012 vs. 0.309 ± 0.012, $n=3$, $p=0.28$). (C) For *Npn1*$^{Sema-}$ mutants no significant alterations in the nerve composition are evident when compared to their control littermates (large diameter axons: 61.96% ± 9.97% vs. 83.37% ± 1.24%, $n=3$, $p=0.10$; small diameter axons: 30.75% ± 11.13% vs. 9.87% ± 1.26%, $n=3$, $p=0.136$; axons per remak bundle: 8.52 ± 0.078 vs. 7.78 ± 0.54, $n=3$, $p=0.31$; *G*-ratio: 0.422 ± 0.058 vs. 0.366 ± 0.016, $n=3$, $p=0.45$).

that leads to secondary bone malformations and deficits in motor behavior and is caused by a dysfunctional innervation due to the loss of motor axons in the *N. radial*. Even though *Npn1*$^{Sema-}$ mutants were also found to have defasciculated motor axons during embryonic development, these animals are not affected to the same extend and only show deficits in complex motor tasks, which they are able to overcome with time. Thus, we demonstrated, that the lack of Sema3A-Npn1 signaling can be largely compensated for while the complete loss of the receptor Npn1 from motor neurons causes severe motor defects in postnatal animals.

Discussion

A number of recent studies have shown the importance of Npn1 for the development of the murine central (Chauvet et al., 2007; Cioni et al., 2013; Piper et al., 2009) and peripheral nervous system (Haupt et al., 2010; Huber et al., 2005; Huettl and Huber, 2011; Huettl et al., 2011; Maden et al., 2012; Roffers-Agarwal and Gammill, 2009; Schwarz et al., 2008). However, the emerging consequences of a missing Npn1 signaling after birth have not been analyzed with the same scrutiny. Thus, in this study the effects of elimination of Npn1 in all motor neurons (*Olig2-Cre*$^{+}$*; Npn1*$^{cond-/-}$) or the complete loss of Sema3A-Npn1 signaling in all cells of the body (*Npn1*$^{Sema-}$) were analyzed in postnatal mice.

Dysfunctional innervation of extensor musculature results in muscle atrophy and bone malformation in Olig2-Cre^{+}*;Npn1*$^{cond-/-}$ *mutants*

A common complication of the wrist drop caused by radial nerve palsy (Reid, 1988) is an atrophy of the affected extensor muscles. Similarly, the depletion of Npn1 from all motor neurons in *Olig2-Cre*$^{+}$*;Npn1*$^{cond-/-}$ mutants causes a wrist drop phenotype that is accompanied by an atrophy of extensor muscles in the affected forelimbs that deteriorates even further during postnatal development. Since denervation is one of the main causes for muscular atrophy (Jackman and Kandarian, 2004) and many motor neuron diseases like amyotrophic lateral sclerosis or progressive motor neuropathy show muscle atrophy as a major symptom (Aguilar et al., 2007; Huettl et al., 2011; Schmalbruch et al., 1991), it is plausible that the embryonic deficits in axon pathfinding and the

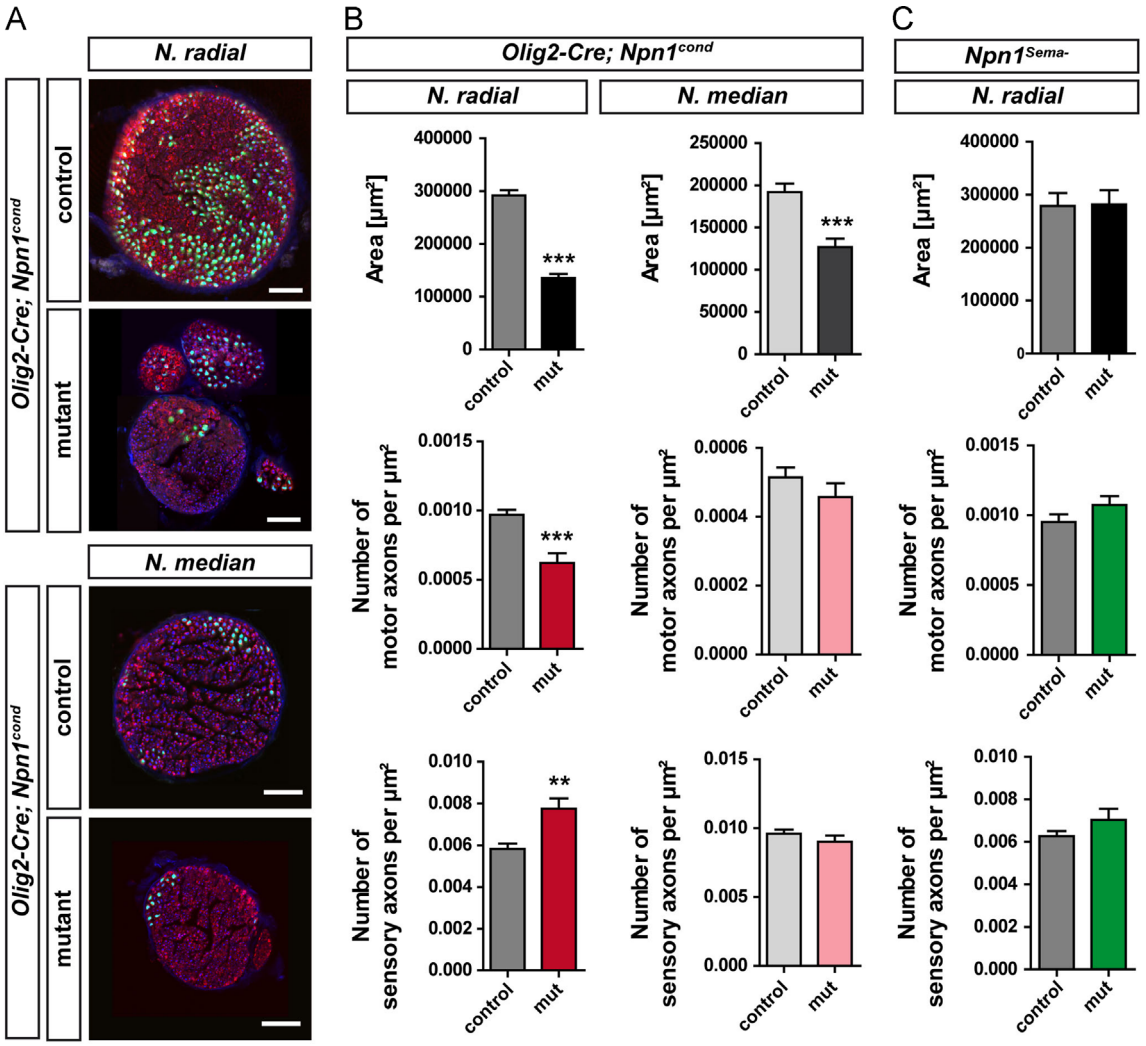

Fig. 4. The number of motor axons is decreased in *Olig2-Cre*$^{+}$*;Npn1*^{cond} mutants. (A) Cross-section of the radial and median nerves from *Olig2-Cre;Npn1*^{cond}*; Hb9::eGFP*$^{+}$ animals after immunohistological staining against myelin basic protein (red), neurofilament (blue) and GFP (green). (B) Analysis of the nerves of *Olig2-Cre;Npn1*^{cond}*; Hb9::eGFP*$^{+}$ animals reveals a significant reduction in the size of the radial nerve in mutants compared to their littermate controls (292100 µm^2 ± 9841 µm^2, $n=7$ vs. 135600 µm^2 ± 8078 µm^2, $n=5$, $p<0.001$). At the same time, the relative number of GFP^{+} motor axons in the radial nerve of mutants is decreased compared to their littermate controls (0.00097 ± 0.000036, $n=7$ vs. 0.00062 ± 0.00007, $n=5$, $p<0.001$). In these nerves the relative number of sensory axons is significantly increased (0.0058 ± 0.00026, $n=7$ vs. 0.0077 ± 0.0005, $n=5$, $p<0.005$). In contrast, the relative number of axons in the median nerve is unchanged (motor axons: 0.000515 ± 0.000028, $n=5$ vs. 0.000457 ± 0.000040, $n=7$, $p=0.23$; sensory axons: 0.00960 ± 0.00030, $n=5$ vs. 0.00902 ± 0.00045, $n=7$, $p=0.27$) even though the size of this nerve is reduced in *Olig2-Cre*$^{+}$*;Npn1*^{cond}*; Hb9::eGFP*$^{+}$ mutants (191700 µm^2 ± 10230 µm^2, $n=7$ vs. 127000 µm^2 ± 9784 µm^2, $n=5$, $p<0.001$). (C) In *Npn1*$^{Sema-}$ mutants the size of the radial nerve shown no significant difference when compared to controls (279000 µm^2 ± 24310 µm^2, $n=3$ vs. 281400 µm^2 ± 27280 µm^2, $n=3$, $p=0.95$). The relative numbers of motor axons (0.00092 ± 0.000054, $n=3$ vs. 0.001074 ± 0.000063, $n=3$, $p=0.08$) and sensory axons (0.006270 ± 0.00025, $n=3$ vs. 0.007033 ± 0.00052, $n=3$, $p=0.21$) remain unchanged when compared to littermate controls. Scale bars: 50 µm.

detected alterations in axonal composition cause innervation deficits in the extensor muscles that result in the observed loss of muscle volume. The functional analysis of the extensor muscle innervation provides additional corroboration for this conclusion, since no activation of the extensor muscles was ever reported in the affected forelimbs of *Olig2-Cre*$^{+}$*;Npn1*$^{cond-/-}$ mice upon electrophysiological stimulation of the *N.radial*, while flexor muscles displayed the expected movements. Embryonic skeletal muscles provide trophic support for motor neurons and thereby control their numbers and survival (Hollyday and Hamburger, 1976; Phelan and Hollyday, 1991). Thus, if extensor muscle atrophy already starts during embryogenesis this may lead to a self-enhancing effect, since reduced levels of trophic support causes programmed cell death in motor neurons which reduces the number of innervating neurons for the affected extensor muscles even more and thereby further acerbates muscle atrophy.

Besides muscle atrophy, also malformations in the structure of the bones of the forepaw were evident in 40 weeks old mice, while newborn pups did not show any abnormalities in skeleton morphology. This might be a secondary effect caused by mechanical misuse due to the observed muscle atrophy since earlier studies in rodent models of spinal muscular atrophy, spinal cord injury or induced focal muscle paralysis show that muscle and nerve dysfunction induce pathological changes in bone volume and composition (Kingery et al., 2003; Shanmugarajan et al., 2009; Warner et al., 2006).

Innervation deficits in Olig2-Cre^{+}*;Npn1*$^{cond-/-}$ *mutants are caused by a loss of motor axons*

This observed posturing defect in the forelimbs of *Olig2-Cre*$^{+}$*; Npn1*^{cond} mutants resembles the limb morphology observed for

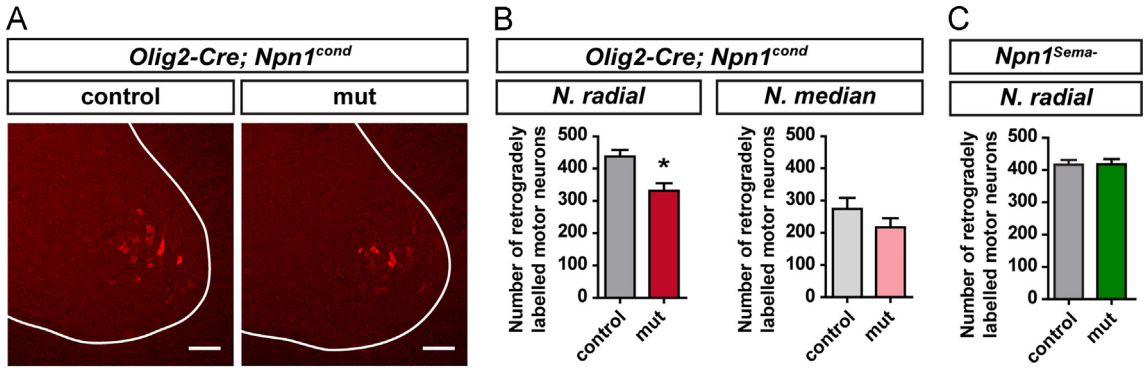

Fig. 5. Retrograde tracing of motor neurons reveals alterations in the radial nerve of *Olig2-Cre*$^{+}$*;Npn1*^{cond} mutants. (A) Retrogradely labeled motor neurons after injection of CTB-Ax555 into the radial nerve of *Olig2-Cre;Npn1*^{cond} animals at the age of 6 weeks. (B) The number of retrogradely traced motor neurons from the radial nerve is significantly lower than in littermate controls (437.3 ± 20.85 vs. 331.3 ± 23.62, $n=3$, $p < 0.05$), while no significant changes are evident after retrograde tracing from the median nerve (280.7 ± 34.07 vs. 217.0 ± 21.57, $n=3$, $p=0.19$). (C) Tracer injection into the radial nerve of *Npn1*$^{Sema-}$ mutants does not result in any changes of the number of retrogradely labeled motor neurons in comparison to their littermate controls (416.5 ± 7.64, $n=4$ vs. 417.3 ± 16.15, $n=3$; $p=0.96$). Scale bars: 100 μm.

claw paw (*clp*) mutant mice which carry an insertion in exon 4 of the Lgi4 gene and show wrists that are flexed towards the body in one or more joints (Bermingham et al., 2006; Henry et al., 1991). In both mouse lines the abnormal posture was not fixed since the paws could be extended passively. The reason for the wrist-drop phenotype in *clp* mutants was found in a malfunctioning innervation of the limbs due to deficits in axonal sorting and myelination of the peripheral nervous system. Closer investigation of the peripheral nerves revealed a general hypomyelination and delayed onset of myelination. Furthermore, large diameter axons were found in a promyelinated state in adult mice until 20 months of age with the size of these axons being noticeably small (Darbas et al., 2004; Henry et al., 1991; Koszowski et al., 1998). Due to the striking similarity of the limb morphology, we analyzed nerves from *Olig2-Cre*$^{+}$*;Npn1*$^{cond-/-}$ mice for myelination deficits. Upon examination of the myelin sheaths of axons from *Olig2-Cre*$^{+}$*;Npn1*$^{cond-/-}$ mice no differences in axon myelination were found. However, a closer investigation of the nerve composition revealed several significant differences. *N. radial* and *N. median* showed a significant decrease in size and the total number of motor and sensory axons was reduced in both nerves. This overall reduction in nerve size is probably the result of the severe deficits in axon fasciculation during embryonic development (Huettl et al., 2011). Since in *Olig2-Cre*$^{+}$*;Npn1*$^{cond-/-}$ mutants all brachial nerves are affected and it is hardly possible to distinguish specific nerve branches this might result in an overall reduction in nerve size. Furthermore, the decreased number of large diameter axons and the relative reduction of GFP^{+} axons in the in the *N. radial* of *Olig2-Cre*$^{+}$*;Npn1*$^{cond-/-}$*; Hb9::eGFP* mice can be explained by a loss of motor axons, which is corroborated by the reduced number of motor neurons that were retrogradely traced from this nerve in the brachial plexus. Also here embryonic development provides an explanation for the observed effects. During embryonic development, axons of the *N. radial* do not appear to reach their target muscles in the dorsal forelimb, since at this side the injection of rhodamin-coupled dextran never led to any motor neurons cell bodies that are labeled by the retrogradely transported tracer (Huettl et al., 2011). Therefore, it is likely that these axons die later due to a lack of trophic support. In contrast, at the ventral side of the limb sufficient axons seem to reach their appropriate target, which might explain why the *N. median* is not affected to the same extent and flexor innervation is still intact in postnatal animals.

Ultrastructural analysis of the nerves also revealed an increased number of axons that are incorporated in Remak bundles, which might suggest impairments in radial sorting. During this process the axon diameter determines the fate of the associating Schwann cells. A large diameter prunes immature Schwann cells to establish a myelin sheath around single axons, while several small diameter axons become incorporated by non-myelinating Schwann cells to form Remak bundles (Garbay et al., 2000; Jessen and Mirsky, 2005). For this process the interaction between axons and Schwann cells is of crucial importance. Since Npn1 expression is maintained in the postnatal spinal cord (De Winter et al., 2006), the missing communication between the receptor Npn1 and a putative interactor on Schwann cells might account for the observed defects in *Olig2-Cre*$^{+}$*;Npn1*$^{cond-/-}$ mice. This notion is corroborated by the reported impairment of Schwann cell migration along cranial nerves in these mice (Huettl and Huber, 2011). Possible Schwann cell-derived binding partners for Npn1 could be an additional Npn1 receptor (Raper, 2000), L1, which is also already known to be involved in axon guidance (Castellani, 2002; Cohen et al., 1998; Nieke and Schachner, 1985), or yet undefined ligands. This is also supported by the finding that in *Npn1*$^{Sema-}$ mice no alterations in myelination or nerve composition were evident, encouraging the idea of a mechanism independent from Sema3A-Npn1 signaling.

Npn1^{Sema-} *mutants can compensate for deficits in axonal wiring*

Even though a wrist-drop was found in *clp* mutants and *Olig2-Cre*$^{+}$*;Npn1*$^{cond-/-}$ mice, both lines show certain differences and variety in the severity of the phenotype. While in *Olig2-Cre*$^{+}$*;Npn1*$^{cond-/-}$ mice the mutation affected only the forepaws, *clp* mutants also displayed impairments in the hindlimbs of more severely affected animals (Henry et al., 1991). These differences in the severity of posturing deficits were also reflected in their behavior. While *clp* mutants revealed significant deficits in general health parameters and overground locomotion (Henry et al., 1991), *Olig2-Cre*$^{+}$*;Npn1*$^{cond-/-}$ showed no such impairments. Only more complex motor skills like balance or motor coordination were affected in these mice. The weakest behavioral phenotype was found in *Npn1*$^{Sema-}$ mice. Here, no posturing deficit was evident and only motor coordination was impaired. Furthermore, these mice were able to improve their performance to wildtype levels from 4 to 12 weeks of age. The observed differences in the three mouse lines may be explained by the results from investigations of the embryonic nervous system. In *Olig2-Cre*$^{+}$*;Npn1*^{cond} mutants, motor axons are defasciculated and the injection of rhodamin-coupled dextran into the ventral side of the forelimb revealed an increased number of axons that were misguided to the opposite side of the limb. However, these defects were never observed in hindlimbs. Therefore, it is not surprising that, in contrast to *clp* mutants, hindlimbs were never affected in these animals. Furthermore, only in *Olig2-Cre*$^{+}$*;Npn1*$^{cond-/-}$ mice a strong reduction of

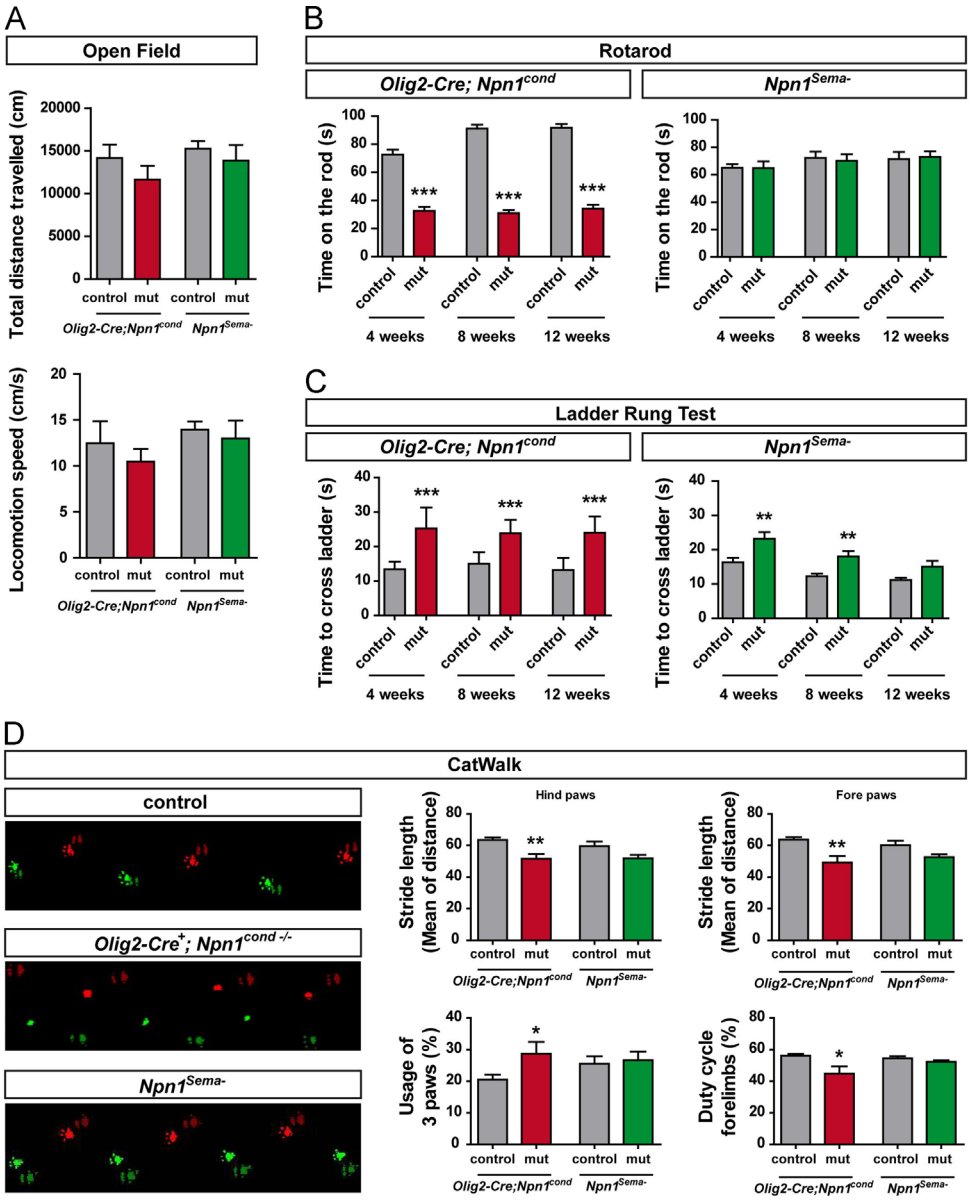

Fig. 6. Motor behavior of *Olig2-Cre;Npn1*^{cond} and *Npn1*$^{Sema-}$ animals. (A) In the open field test the total traveling distance is similar for *Olig2-Cre*$^{+}$*;Npn1*^{cond} mutants (14150 ± 1576 cm vs. 11640 ± 161 cm, $p=0.29$, $n=7$) and *Npn1*$^{Sema-}$ mutants (15245 ± 890.5 vs. 13839 ± 1834, $p=0.19$, $n=12$) compared to their littermate controls. Also the locomotion speed does not show significant differences for *Olig2-Cre*$^{+}$*;Npn1*^{cond} mutants (12.45 cm/s ± 2.42 cm/s vs. 10.48 cm/s ± 1.37cm/s, $p=0.48$, $n=7$) or *Npn1*$^{Sema-}$ mutants (13.93 cm/s ± 0.91 cm/s vs. 13.01 cm/s ± 1.92 cm/s, $p=0.67$, $n=12$). (B) On the rotarod *Olig2-Cre*$^{+}$*;Npn1*^{cond} mutants show a significantly decreased endurance at each timepoint (4 weeks: 32.53 ± 2.85 s; 8 weeks: 31.00 ± 2.26 s; 12 weeks: 34.17 ± 2.74 s; $n=10$) compared to their littermate controls (4 weeks: 72.60 ± 3.561 s; 8 weeks: 91.20 ± 2.66 s; 12 weeks: 91.70 ± 2.67 s; $n=10$) ($p<0.001$ for each timepoint). In contrast, for *Npn1*$^{Sema-}$ mice no difference is detectable between mutants (4 weeks: 64.89 ± 4,88 s; 8 weeks: 70.14 ± 4.78 s; 12 weeks: 72.97 ± 4.01 s; $n=10$) and control animals (4 weeks: 65.11 ± 2.70 s; 8 weeks: 72.36 ± 4.55 s; 12 weeks: 71.33 ± 5.38 s; $n=10$) at each timepoint (4weeks: $p=0.75$; 8 weeks: $p=0.91$; 12 weeks: 0.87). (C) In the ladder rung test *Olig2-Cre*$^{+}$*;Npn1*^{cond} mutants perform significantly worse than their littermate controls with no improvement during postnatal development (4 weeks: 13.44 ± 0.89 s vs. 25.26 ± 2.39 s; 8 weeks: 15.03 ± 1.05 s vs. 23.83 ± 1.23 s; 12 weeks: 13.17 ± 1.11 s vs. 24.00 ± 1.49 s; $n=10$; $p<0.001$ for each timepoint). *Npn1*$^{Sema-}$ mutants show a significantly worse performance at 4 and 8 weeks of age (4 weeks: 16.31 ± 1.39 s vs. 23.22 ± 1.90 s, $p<0.01$; 8 weeks: 12.24 ± 0.81 s vs. 18.00 ± 1.58 s; $n=10$; $p<0.01$), however, at 12 weeks of age they reveal improved coordinative skills and perform at similar levels as their control littermates (11.14 ± 0.67 s vs. 15.00 ± 1.73 s; $n=10$; $p<0.1$). (D) The Catwalk analysis reveals significant alterations in the stride length of forepaws (63.73 ± 1.48, $n=9$ vs. 49.15 ± 4.19, $n=8$, $p<0.005$) and hindpaws (63.53 ± 1.56, $n=9$ vs. 51.54 ± 3.18, $n=8$; $p<0.005$), the usage of three paws (20.44% ± 1.67%, $n=9$ vs. 28.72% ± 3.75%, $n=7$; $p<0.05$) and the duty cycle of the forelimbs (56.14 ± 1.23, $n=9$ vs. 44.86 ± 4.50, $n=8$; $p<0.05$) for *Olig2-Cre*$^{+}$*;Npn1*^{cond} mutants compared to their littermate controls. In contrast, *Npn1*$^{Sema-}$ mutants show no changes in these parameters (stride length of forepaws: 60.18 ± 2.83, $n=9$ vs. 52.65 ± 1.833, $n=5$, $p=0.090$; stride length of hindpaws: 59.61 ± 2.88, $n=9$ vs. 51.92 ± 2.09, $n=5$; $p=0.093$; usage of three paws: 25.54% ± 2.34%, $n=9$ vs. 26.64% ± 2.756%, $n=5$; $p=0.77$; duty cycle of the forelimbs: 54.45 ± 1.39, $n=9$ vs. 52.27 ± 0.93, $n=5$; $p=0.30$).

the distal advancement of motor projections into the forelimb during embryonic development was reported. In addition, axons of the radial branch do not extend far enough to reach their target zones in the dorsal side of the forelimb (Huettl et al., 2011). This might explain the differences to the less affected *Npn1*$^{Sema-}$ mutants, since here axons are defasciculated and reveal pathfinding deficits, however in these animals the axons enter the limb prematurely and show longer projections in the embryonic state. Thus, the number of axons that still reach their correct target muscles might be enough to allow for a sufficient innervation of the musculature. In this case, fasciculation deficits might be compensated to a certain extent, since aberrant motor projections are pruned during normal development (Vanderhaeghen and Cheng, 2010). In addition, supernumerary motor neurons are reduced

during the period of naturally occurring cell death due to a lack of trophic support (Hollyday and Hamburger, 1976; Phelan and Hollyday, 1991), which might contribute to the compensatory effects that help *Npn1*$^{Sema-}$ mutants to overcome their developmental axon guidance deficits.

In conclusion, our data suggest that the loss of Npn1 from motor neurons causes a wrist-drop in the forelimbs of *Olig2-Cre*$^{+}$*;Npn1*$^{cond-/-}$ mice due to a reduced number of dorsally projecting motor neurons and the resulting deficient innervation of the extensor muscles. The phenotype is accompanied by muscle atrophy, bone malformation, and deficits in skilled motor behavior. The loss of Sema3A-Npn1 signaling in motor neurons is, however, not the only molecular cause for the described effects, since *Npn1*$^{Sema-}$ mutants do not reveal the same deficits. Therefore, it is likely that Npn1 is able to interact with additional binding partners like VEGF, L1 or other yet unknown ligands to control sensory-motor circuit wiring and that this interaction initiates compensatory mechanisms that account for the minor disturbances in *Npn1*$^{Sema-}$ mutants.

Acknowledgments

This work has been funded by the International Foundation for Research in Paraplegia (grant P96 to ABH), the Helmholtz Portfolio Theme “Supercomputing and Modeling for the Human Brain” (SMHB), and by the German Federal Ministry of Education and Research to the GMC (Infrafrontier grant 01KX1012).

We thank R.E. Huettl, M.A. Castiblanco Urbina, C. Haupt and G. Luxenhofer for scientific discussions and acknowledge J. Maetsch, A. Mantik, J. Langhoff, D. Picht and M. Miller for technical assistance.

Appendix A. Supporting information

Supplementary data associated with this article can be found in the online version at http://dx.doi.org/10.1016/j.ydbio.2014.11.024.

References

Baatz, M., Arini, N., Schape, A., Binnig, G., Linssen, B., 2006. Object-oriented image analysis for high content screening: detailed quantification of cells and sub cellular structures with the Cellenger software. Cytom. Part A: J. Int. Soc. Anal. Cytol. 69, 652–658.

Baatz, M., Zimmermann, J., Blackmore, C.G., 2009. Automated analysis and detailed quantification of biomedical images using Definiens Cognition Network Technology. Comb. Chem. High Throughput Screen. 12, 908–916.

Bermingham Jr., J.R., Shearin, H., Pennington, J., O'Moore, J., Jaegle, M., Driegen, S., van Zon, A., Darbas, A., Ozkaynak, E., Ryu, E.J., et al., 2006. The claw paw mutation reveals a role for Lgi4 in peripheral nerve development. Nat. Neurosci. 9, 76–84.

Castellani, V., 2002. The function of neuropilin/L1 complex. Adv. Exp. Med. Biol. 515, 91–102.

Chauvet, S., Cohen, S., Yoshida, Y., Fekrane, L., Livet, J., Gayet, O., Segu, L., Buhot, M.C., Jessell, T.M., Henderson, C.E., et al., 2007. Gating of Sema3E/PlexinD1 signaling by neuropilin-1 switches axonal repulsion to attraction during brain development. Neuron 56, 807–822.

Cioni, J.M., Telley, L., Saywell, V., Cadilhac, C., Jourdan, C., Huber, A.B., Huang, J.Z., Jahannault-Talignani, C., Ango, F., 2013. SEMA3A signaling controls layer-specific interneuron branching in the cerebellum. Curr. Biol.: CB 23, 850–861.

Cohen, N.R., Taylor, J.S., Scott, L.B., Guillery, R.W., Soriano, P., Furley, A.J., 1998. Errors in corticospinal axon guidance in mice lacking the neural cell adhesion molecule L1. Curr. Biol.: CB 8, 26–33.

Darbas, A., Jaegle, M., Walbeehm, E., van den Burg, H., Driegen, S., Broos, L., Uyl, M., Visser, P., Grosveld, F., Meijer, D., 2004. Cell autonomy of the mouse claw paw mutation. Dev. Biol. 272, 470–482.

De Winter, F., Vo, T., Stam, F.J., Wisman, L.A., Bar, P.R., Niclou, S.P., van Muiswinkel, F.L., Verhaagen, J., 2006. The expression of the chemorepellent Semaphorin 3A is selectively induced in terminal Schwann cells of a subset of neuromuscular synapses that display limited anatomical plasticity and enhanced vulnerability in motor neuron disease. Mol. Cell. Neurosci. 32, 102–117.

Dessaud, E., Yang, L.L., Hill, K., Cox, B., Ulloa, F., Ribeiro, A., Mynett, A., Novitch, B.G., Briscoe, J., 2007. Interpretation of the sonic hedgehog morphogen gradient by a temporal adaptation mechanism. Nature 450, 717–720.

Egea, J., Klein, R., 2007. Bidirectional Eph-ephrin signaling during axon guidance. Trends Cell Biol. 17, 230–238.

Garbay, B., Heape, A.M., Sargueil, F., Cassagne, C., 2000. Myelin synthesis in the peripheral nervous system. Prog. Neurobiol. 61, 267–304.

Glasl, L., Kloos, K., Giesert, F., Roethig, A., Di Benedetto, B., Kuhn, R., Zhang, J., Hafen, U., Zerle, J., Hofmann, A., et al., 2012. Pink1-deficiency in mice impairs gait, olfaction and serotonergic innervation of the olfactory bulb. Exp. Neurol. 235, 214–227.

(Gonzalez de) Aguilar, J.L., Echaniz-Laguna, A., Fergani, A., Rene, F., Meininger, V., Loeffler, J.P., Dupuis, L., 2007. Amyotrophic lateral sclerosis: all roads lead to Rome. J. Neurochem. 101, 1153–1160.

Greene, E., 1963. Transactions of the American Philosophical Society: Anatomy of the Rat. Hafner Publishing Company, New York and London.

Gross, T.S., Poliachik, S.L., Prasad, J., Bain, S.D., 2010. The effect of muscle dysfunction on bone mass and morphology. J. Musculoskelet. Neuronal Interact. 10, 25–34.

Gu, C., Rodriguez, E.R., Reimert, D.V., Shu, T., Fritzsch, B., Richards, L.J., Kolodkin, A.L., Ginty, D.D., 2003. Neuropilin-1 conveys semaphorin and VEGF signaling during neural and cardiovascular development. Dev. Cell 5, 45–57.

Haupt, C., Kloos, K., Faus-Kessler, T., Huber, A.B., 2010. Semaphorin 3A-Neuropilin-1 signaling regulates peripheral axon fasciculation and pathfinding but not developmental cell death patterns. Eur. J. Neurosci. 31, 1164–1172.

Henry, E.W., Eicher, E.M., Sidman, R.L., 1991. The mouse mutation claw paw: forelimb deformity and delayed myelination throughout the peripheral nervous system. J. Hered. 82, 287–294.

Hensch, T.K., 2005. Critical period plasticity in local cortical circuits. Nat. Rev.. Neurosci. 6, 877–888.

Hollyday, M., Hamburger, V., 1976. Reduction of the naturally occurring motor neuron loss by enlargement of the periphery. J. Comp. Neurol. 170, 311–320.

Huber, A.B., Kania, A., Tran, T.S., Gu, C., De Marco Garcia, N., Lieberam, I., Johnson, D., Jessell, T.M., Ginty, D.D., Kolodkin, A.L., 2005. Distinct roles for secreted semaphorin signaling in spinal motor axon guidance. Neuron 48, 949–964.

Huber, A.B., Kolodkin, A.L., Ginty, D.D., Cloutier, J.F., 2003. Signaling at the growth cone: ligand–receptor complexes and the control of axon growth and guidance. Ann. Rev. Neurosci. 26, 509–563.

Huettl, R.E., Huber, A.B., 2011. Cranial nerve fasciculation and Schwann cell migration are impaired after loss of Npn-1. Dev. Biol. 359, 230–241.

Huettl, R.E., Soellner, H., Bianchi, E., Novitch, B.G., Huber, A.B., 2011. Npn-1 contributes to axon-axon interactions that differentially control sensory and motor innervation of the limb. PLoS Biol. 9, e1001020.

Jackman, R.W., Kandarian, S.C., 2004. The molecular basis of skeletal muscle atrophy. Am. J. Physiol. Cell Physiol. 287, C834–C843.

Jessen, K.R., Mirsky, R., 2005. The origin and development of glial cells in peripheral nerves. Nat. Rev. Neurosci. 6, 671–682.

Jolesz, F., Sreter, F.A., 1981. Development, innervation, and activity-pattern induced changes in skeletal muscle. Annu. Rev. Physiol. 43, 531–552.

Kao, T.J., Law, C., Kania, A., 2012. Eph and ephrin signaling: lessons learned from spinal motor neurons. Sem. Cell Dev. Biol. 23, 83–91.

Kingery, W.S., Offley, S.C., Guo, T.Z., Davies, M.F., Clark, J.D., Jacobs, C.R., 2003. A substance P receptor (NK1) antagonist enhances the widespread osteoporotic effects of sciatic nerve section. Bone 33, 927–936.

Kolodkin, A.L., Tessier-Lavigne, M., 2011. Mechanisms and molecules of neuronal wiring: a primer. Cold Spring Harb. Persp. Biol., 3.

Koszowski, A.G., Owens, G.C., Levinson, S.R., 1998. The effect of the mouse mutation claw paw on myelination and nodal frequency in sciatic nerves. J. Neurosci.: Off. J. Soc. Neurosci. 18, 5859–5868.

Kramer, E.R., Knott, L., Su, F., Dessaud, E., Krull, C.E., Helmbacher, F., Klein, R., 2006. Cooperation between GDNF/Ret and ephrinA/EphA4 signals for motor–axon pathway selection in the limb. Neuron 50, 35–47.

Lichtman, J.W., Colman, H., 2000. Synapse elimination and indelible memory. Neuron 25, 269–278.

Maden, C.H., Gomes, J., Schwarz, Q., Davidson, K., Tinker, A., Ruhrberg, C., 2012. NRP1 and NRP2 cooperate to regulate gangliogenesis, axon guidance and target innervation in the sympathetic nervous system. Dev. Biol. 369, 277–285.

Metz, G.A., Schwab, M.E., 2004. Behavioral characterization in a comprehensive mouse test battery reveals motor and sensory impairments in growth-associated protein-43 null mutant mice. Neuroscience 129, 563–574.

Nieke, J., Schachner, M., 1985. Expression of the neural cell adhesion molecules L1 and N-CAM and their common carbohydrate epitope L2/HNK-1 during development and after transection of the mouse sciatic nerve. Differ.; Res. Biol. Divers. 30, 141–151.

Phelan, K.A., Hollyday, M., 1991. Embryonic development and survival of brachial motoneurons projecting to muscleless chick wings. J. Comp. Neurol. 311, 313–320.

Piper, M., Plachez, C., Zalucki, O., Fothergill, T., Goudreau, G., Erzurumlu, R., Gu, C., Richards, L.J., 2009. Neuropilin 1-Sema signaling regulates crossing of cingulate pioneering axons during development of the corpus callosum. Cereb. cCortex 19 (Suppl 1), s11–s21.

Plumier, J.C., Hopkins, D.A., Robertson, H.A., Currie, R.W., 1997. Constitutive expression of the 27-kDa heat shock protein (Hsp27) in sensory and motor neurons of the rat nervous system. J. Comp. Neurol. 384, 409–428.

Raper, J.A., 2000. Semaphorins and their receptors in vertebrates and invertebrates. Curr. Opin. Neurobiol. 10, 88–94.

Reid, R.L., 1988. Radial nerve palsy. Hand Clin. 4, 179–185.

Roffers-Agarwal, J., Gammill, L.S., 2009. Neuropilin receptors guide distinct phases of sensory and motor neuronal segmentation. Development 136, 1879–1888.

Schmalbruch, H., Jensen, H.J., Bjaerg, M., Kamieniecka, Z., Kurland, L., 1991. A new mouse mutant with progressive motor neuronopathy. J. Neuropathol. Exp. Neurol. 50, 192–204.

Schwarz, Q., Vieira, J.M., Howard, B., Eickholt, B.J., Ruhrberg, C., 2008. Neuropilin 1 and 2 control cranial gangliogenesis and axon guidance through neural crest cells. Development 135, 1605–1613.
Shanmugarajan, S., Tsuruga, E., Swoboda, K.J., Maria, B.L., Ries, W.L., Reddy, S.V., 2009. Bone loss in survival motor neuron (Smn(-/-) SMN2) genetic mouse model of spinal muscular atrophy. J. Pathol. 219, 52–60.
Udina, E., Furey, M., Busch, S., Silver, J., Gordon, T., Fouad, K., 2008. Electrical stimulation of intact peripheral sensory axons in rats promotes outgrowth of their central projections. Exp. Neurol. 210, 238–247.
Vanderhaeghen, P., Cheng, H.J., 2010. Guidance molecules in axon pruning and cell death. Cold Spring Harb. Persp. Biol. 2, a001859.
Warner, S.E., Sanford, D.A., Becker, B.A., Bain, S.D., Srinivasan, S., Gross, T.S., 2006. Botox induced muscle paralysis rapidly degrades bone. Bone 38, 257–264.
Wichterle, H., Lieberam, I., Porter, J.A., Jessell, T.M., 2002. Directed differentiation of embryonic stem cells into motor neurons. Cell 110, 385–397.
Yu, W.M., Feltri, M.L., Wrabetz, L., Strickland, S., Chen, Z.L., 2005. Schwann cell-specific ablation of laminin gamma1 causes apoptosis and prevents proliferation. J. Neurosci. 25, 4463–4472.
Zadicario, P., Avni, R., Zadicario, E., Eilam, D., 2005. 'Looping' – an exploration mechanism in a dark open field. Behav. Brain Res. 159, 27–36.